UCLA
UCLA Previously Published Works

Title
Landslides on Ceres: Diversity and Geologic Context

Permalink
https://escholarship.org/uc/item/7zz083q7

Journal
Journal of Geophysical Research Planets, 124(12)

ISSN
2169-9097

Authors
Duarte, KD
Schmidt, BE
Chilton, HT
et al.

Publication Date
2019-12-01

DOI
10.1029/2018je005673

Peer reviewed

Landslides on Ceres: Diversity and Geologic Context

K. D. Duarte[1], B. E. Schmidt[1] iD, H. T. Chilton[1] iD, K. H. G. Hughson[1,2] iD, H. G. Sizemore[3] iD, K. L. Ferrier[1] iD, J. J. Buffo[1], J. E. C. Scully[4] iD, A. Nathues[5], T. Platz[5] iD, M. Landis[6,7] iD, S. Byrne[6], M. Bland[8] iD, C. T. Russell[2] iD, and C. A. Raymond[4] iD

[1]School of Earth and Atmospheric Sciences, Georgia Institute of Technology, Atlanta, GA, USA, [2]Institute of Geophysics and Planetary Physics, University of California, Los Angeles, CA, USA, [3]Planetary Science Institute, Tucson, AZ, USA, [4]Jet Propulsion Laboratory, California Institute of Technology, Pasadena, CA, USA, [5]Max-Planck Institute for Solar System Research, Katlenburg-Lindau, Germany, [6]Lunar and Planetary Laboratory, University of Arizona, Tucson, AZ, USA, [7]Now at Boulder Laboratory for Atmospheric and Space Physics, University of Colorado Boulder, Boulder, CO, USA, [8]USGS, Flagstaff, AZ, USA

Abstract Landslides are among the most widespread geologic features on Ceres. Using data from Dawn's Framing Camera, landslides were previously classified based upon geomorphologic characteristics into one of three archetypal categories, Type 1(T1), Type 2 (T2), and Type 3 (T3). Due to their geologic context, variation in age, and physical characteristics, most landslides on Ceres are, however, intermediate in their morphology and physical properties between the archetypes of each landslide class. Here we describe the varied morphology of individual intermediate landslides, identify geologic controls that contribute to this variation, and provide first-order quantification of the physical properties of the continuum of Ceres's surface flows. These intermediate flows appear in varied settings and show a range of characteristics, including those found at contacts between craters, those having multiple trunks or lobes; showing characteristics of both T2 and T3 landslides; material slumping on crater rims; very small, ejecta-like flows; and those appearing inside of catenae. We suggest that while their morphologies can vary, the distribution and mechanical properties of intermediate landslides do not differ significantly from that of archetypal landslides, confirming a link between landslides and subsurface ice. We also find that most intermediate landslides are similar to Type 2 landslides and formed by shallow failure. Clusters of these features suggest ice enhancement near Juling, Kupalo and Urvara craters. Since the majority of Ceres's landslides fall in the intermediate landslide category, placing their attributes in context contributes to a better understanding of Ceres's shallow subsurface and the nature of ground ice.

Plain Language Summary Previously, three distinct types of landslides on Ceres, Type 1 (T1), Type 2 (T2), and Type 3 (T3), were identified and classified by their shapes and locations, but most landslides on Ceres do not fall cleanly into those categories based on shape alone. We have analyzed these intermediate landslides to further describe the continuum of flows seen on Ceres. Here, we study their intrinsic properties to gain a greater understanding of Ceres's subsurface properties. Overall, the locations, shapes, and properties of these landslides on Ceres appear to be influenced by ice contained within Ceres's surface and subsurface materials and suggest local ice enhancement is present in some regions, such as near Juling, Kupalo, and Urvara craters.

1. Introduction

After impact craters, landslides are the most numerous geologic features found on Ceres, appearing in over 20% of craters larger than 10 km in diameter and numbering ~170 in total after comprehensive surveys of data through Dawn's Low Altitude Mapping Orbit (LAMO, ~35-m/pixel resolution). Landslides occur largely associated with craters, probably since these are the primary source of topography on Ceres. These features are globally distributed, with an equator to pole gradient in morphology (Buczkowski et al., 2016; Schmidt et al., 2017, Figure 1). Type 1 (T1) landslides are characterized by thick trunks and prominent distal toes, suggesting the occurrence of non-Newtonian flow where the ice content is great enough (Schmidt et al., 2017) and are predominantly found above 50° latitude where shallow ice is stable. Broad, sheeted Type 2 (T2) flows are found across the surface but are concentrated below 50° latitude and have a much longer run-out length than T1 flows suggesting they are mobilized by melted ice (Schmidt et al., 2017). Cuspate, sheeted flows designated as Type 3 (T3) landslides are found at

Hughson, H. G. Sizemore, J. J. Buffo, J. E. C. Scully

Project administration: B. E. Schmidt, A. Nathues, C. T. Russell, C. A. Raymond
Resources: B. E. Schmidt, A. Nathues, T. Platz, C. T. Russell, C. A. Raymond
Supervision: B. E. Schmidt
Validation: B. E. Schmidt
Writing - original draft: K. D. Duarte, B. E. Schmidt
Writing – review & editing: K. D. Duarte, B. E. Schmidt, K. H. G. Hughson, H. G. Sizemore, J. E. C. Scully, A. Nathues, M. Landis, S. Byrne, C. T. Russell, C. A. Raymond

middle to low latitudes either on the rims or within the ejecta blankets of young, large impacts, which suggests that these may actually be fluidized or fluidized ejecta (Schmidt et al., 2017; Hughson et al., 2019). Figure 2 shows examples of all three canonical feature types.

Schmidt et al. (2017) argued that subsurface ground ice plays a role in mobilizing landslides, based on analysis of the landslides' global distribution (Buczkowski et al., 2016), geomorphological characteristics and simple flow geometry arguments. Alongside other evidence for ice (Bland et al., 2016; Combe et al., 2016, 2017; Hayne & Aharonson, 2015; Landis et al., 2017; Nathues, Platz, Hoffmann, et al., 2017; Prettyman et al., 2017; Schorghofer et al., 2016), landslides are consistent with a global ground ice table accessible by shallow geologic processes. In fact, the first direct detection of ice on Ceres was in Oxo crater (Combe et al., 2016) near a T1 landslide. Five of the nine direct spectral ice detections on Ceres (Combe et al., 2017) occur either on crater rims that produce landslides or on landslides themselves. Formisano et al. (2018) have characterized an ice-rich rim in Juling crater that is the largest ice exposure found to date on Ceres and that is associated with a T1 landslide with rock-glacier type morphology.

Whereas Schmidt et al. (2017) focused on global characteristics of morphology and transport distance across all landslide deposits, Chilton et al. (2019) undertook a detailed characterization of archetypal T1 and T2 landslides and made quantitative estimates of friction and failure behavior. They utilized two approaches to estimate effective coefficients of friction for the flows, constrained failure mechanics via the relationship of the area of failure scars and the volume of deposits and further refined the differences in mechanical behavior between landslide types. Chilton et al. (2019) concluded that a layered subsurface consisting of an upper surface layer of ice-poor clay material overlaying ice-rich material below could explain the differences in material failure between the T1 (self-similar scaling) and T2 (depth-limited failure) landslides. They also showed that the equator-pole trend in the distribution of landslides was mostly preserved even when only the type examples classified as T1 and T2 landslides are considered.

Chilton et al. (2019) focused on 32 landslides that best represented the three classes (T1, T2, and T3) in order to understand how morphology and mechanics could be linked. Their study required high-resolution observations where the landslide deposits and failure scars were clearly visible and where Dawn topographic data had sufficient resolution to measure the volume of both the deposits and scars. The morphologies of 115 of the other landslides were complicated by either their geographical setting or observational circumstance; thus, they did not directly fit the Chilton et al. (2019) analysis criteria. Here, we identify these as members of the continuum of Cerean landslides with morphologies intermediate between the type examples of the T1, T2, and T3 classifications and characterize them using morphological and geometric measures.

2. Landslides in Broader Geologic Context

Expanding on the work of Schmidt et al. (2017), we have updated our catalog of identified landslides, eliminating some features that were ambiguous at higher resolution or under several viewing geometries and adding newly identified features, particularly those found in the regions between impact craters. This catalog of landslides, including the T1 and T2 archetypes analyzed by Chilton et al. (2019), T3 landslides identified by Schmidt et al. (2017), and the flows described here as "intermediate" are plotted on a global map of Ceres in Figure 1. We examined calibrated Framing Camera images (Schröder et al., 2013, 2014; Roatsch et al., 2017) from Dawn's LAMO, and topographic data (vertical accuracy ~10 m) from the stereophotogrammetric digital terrain model of Ceres (Preusker et al., 2016). The image resolution is nearly uniform across the body during this orbit, with near global coverage at ~35 m/pixel for the clear filter images analyzed here. These provided higher resolution spatial and topographic information than was available to Schmidt et al. (2017). Utilizing the classification parameters laid out in Schmidt et al. (2017) pertaining to the presence of distinctive distal toes and thick trunks (T1), thin and long run-out deposits (T2), or cuspate, sheeted flows (T3), we were able to constrain the T1, T2, and T3 groups to a greater, more precise extent, leaving us with a continuum group of intermediate landslides. We identified 13 T1, 29 T2, 13 T3, and 115 intermediate features. The intermediate landslides exhibit an array of atypical behaviors not accommodated by the T1, T2, and T3 classifications. Some examples of this variety of behaviors includes features that are associated with crater wall failure likely initiated by a nearby impact, those having multiple lobes and trunks, those with fluidized ejecta appearance and overlap with the analysis of Hughson et al. (2019), and those that form in
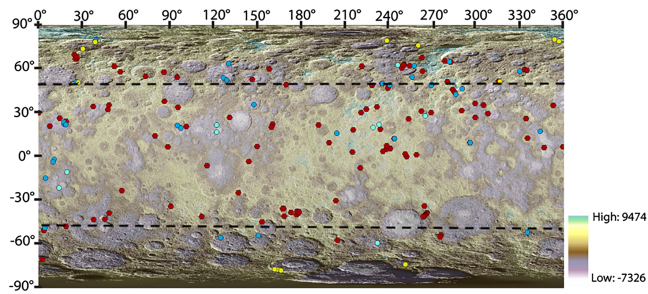
Figure 1. Ceres topography, after Preusker et al. (2016), overlain with the locations of landslides from this study and previous work. The classifications are an update relative to Schmidt et al. (2017). Each color represents a different class of landslide; T1 are given in yellow, T2 are in blue, T3 are in cyan, and the features described here with intermediate properties are indicated by red. Dotted lines indicate 50° latitudinal designation point.

locations not within impact craters. We also refined our measurements of the height versus length ratio (H/L) for most flows with higher-resolution data than was previously available and by averaging multiple topographic profiles taken across each flow.

Landslides are present at all latitudes on Ceres and occur in the context of a number of geological features. These varied provenances contribute to both the morphology and size of landslides, creating a continuum of intermediate behaviors between the T1, T2, and T3 feature archetypes. The intermediate landslides present an opportunity for comparative study, both between archetype Cerean features, and relative to landslides on other planetary bodies. Here we describe some of the variety of intermediate landslides on Ceres, their connection to other geomorphological features, and associations with spectroscopic detections of surface ice.

2.1. "Contact Crater" Landslides

A common setting for landslides is at the contact between the rims of two similarly sized craters, shown in Figure 3 and Table 1. In most of these contact crater flows, where an impact occurs either on the rim of an older crater, or very near it, the rim of the older crater appears to fail, creating a landslide that flows onto the floor of the older crater. Most contact crater flows appear to have thick deposits with distinct distal toes and are morphologically similar to T1 flows in this respect (Figures 3a and 3b, Table 1 below, and supporting information). Because of their setting, it seems likely that contact crater landslides were initiated during the second impact, but they are distinct from ejecta. In general, the largest T1 flows also initiate from impacts into existing crater rims; however, these only initiate from very small impacts high onto the rim of older craters and are confined to the polar regions. Contact crater flows occur at the contacts between similarly sized impacts and the only instances we observe so far are equatorward of 60° latitude (Table 1), whereas T1 flows are found near the poles (e.g., Buczkowski et al., 2016) and do not occur at contact points between large or similarly sized craters (Schmidt et al., 2017). Further, contact crater flows do not have the long tongue-like shapes that T1 landslides generally possess, and in most cases lack longitudinal furrows along their trunks parallel to the direction of motion (Figures 3a and 3b), which characterize T1 flows. Some T1 flows have multiple lobes, whereas contact crater flows always exhibit a single trunk. Despite these morphological differences, both contact craters flows and T1 landslides exhibit deep failure demonstrated by their prominent failure scarps and thick deposits. To our knowledge, the morphology of both T1 and contact crater flows has only been identified on Ceres, which may be related to the unique mechanical structure of Ceres's regolith and shallow subsurface (Chilton et al., 2019).

2.2. Multilobed Landslides

Multilobe features occur in several locations on Ceres (Figure 4). Multiple lobed failures are those in which an initial landslide occurred and was subsequently overprinted by another flow lobe. We see this
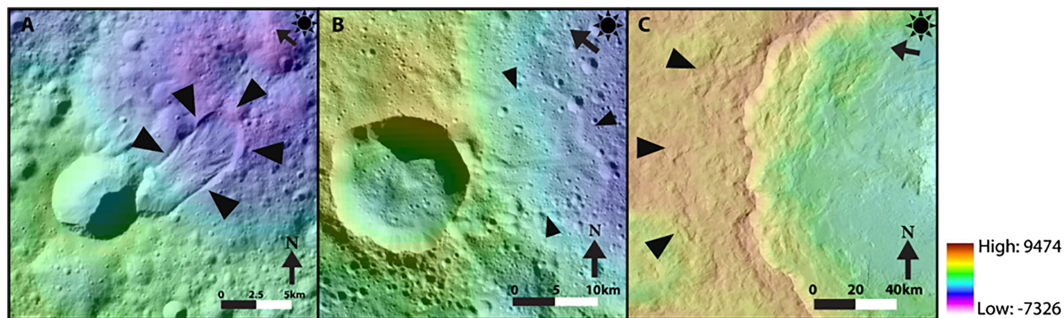
Figure 2. Examples of typical landslides of each class. Color indicates topography in meters. Bold triangles indicate the margin of the landslide. (a) [50.804°, 27.326°], Type 1 landslides exhibit lobate, tongue-shaped morphology, with a well-defined toe. (b) [−48.723°,4.457°], Type 2 landslides have a thin, sheet-like structure, distinctive toe, and long run-out length. (c) [22.061°, −126.711°], Type 3 landslides are cuspate and sheeted, characteristic of fluidized appearing ejecta (Hughson et al., 2019).
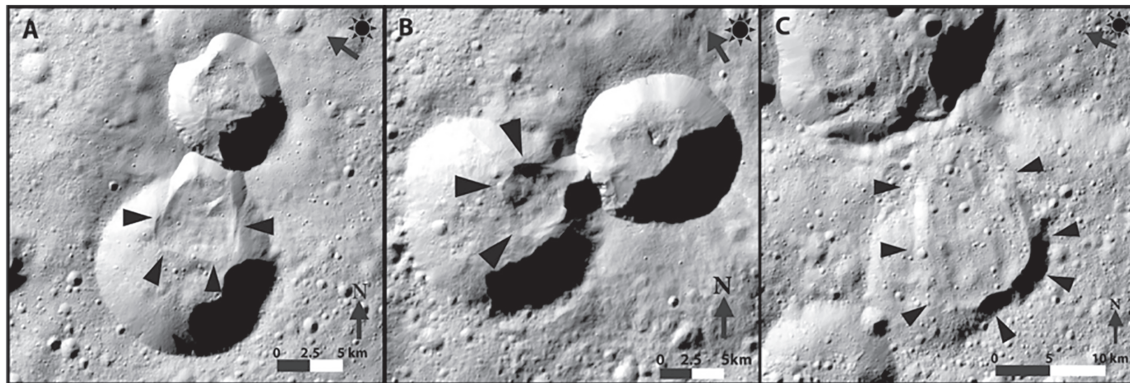
Figure 3. Contact crater landslides are formed at the contact point between the rim of an older crater with a superposed younger crater. (a) [57.819°, 86,110°] A defined scar, rounded toe, and thicker deposit is present, resembling a T1 flow. Rim failure on the northern and southern craters is prevalent. Ejecta from the newer impact is seen on the rim of the southern crater, but the landslide is much thicker and more well defined than ejecta. The landslide also lacks longitudinal furrows and has a smoother deposit surface than most T1 features. (b) [58.153°, 56.327°] A contact crater landslide with defined scar and rounded, thick toe, and a short run-out length into the older crater, resembling a T1 flow. (c) [54.359°, 95.147°] In this image, a thinner landslide with a long run-out length and morphology resembling a T2 landslide flows into an older crater, yet it has a more rounded toe like a traditional T1 landslide. Unlike in (a) and (b), this flow does not represent the complete collapse of the crater rim. In this case, the steep scarp to the south of the flow may have limited the runout of the feature and causing otherwise T2-like feature to have T1 attributes.

type of behavior in both T1 (Figure 4a) and T2 (Figure 4b) landslides, including those associated with fluidized appearing ejecta (Figure 4b). The stratigraphic juxtaposition of the overprinting flows suggests that in some cases postimpact failure may be an extended process, with ongoing modification, rather than forming entirely at the time of impact. Even in some contact craters (Figure 4c), it is possible for several overprinting flows to occur in the same crater, sourced from the same rim. While multilobe flows are generally easy to identify, the juxtaposition of lobes can make measuring and characterizing material parameters of these features difficult. For example, overprinting of flows could create distal toes that are thicker than a single flow would create. Crosscutting relationships likely affect basal conditions and flow mobility, since some lobes formed over crater floor materials, and others formed over older landslide deposits. In some cases, talus materials superpose landslide materials, obscuring the detailed morphology. Thus, although the morphology of these flows is not difficult to classify, their failure behavior is much more difficult to interpret due to obscuration of older scars and older floor deposits by more recent flows, making analysis such as that performed in Chiton et al (this issue) impossible.

2.3. "Ejecta-Landslide" Flows

We also observe distinct landslide features with evident distal toes sourced from craters that host T3 features or that form within materials associated with T3 fluidized appearing ejecta (Figure 5a). The distinct toe and thin deposit of these T2–T3 ejecta-landslide flows are visually similar to T2 types and often overprint T3 landslides or ejecta (Figures 5b and 5c), indicating formation after the initial flow is emplaced. This type of flow, however, lacks a visible scar, which is more akin to T3 flows than T2 flows. In some cases, multiple flow lobes overlap one another, so it is unclear if the thick distal toes arise from a single flow or from multiple overlapping flows interacting. Intermediate T2–T3 flows are often also found in depressions near the source of T3 landslide or fluidized appearing ejecta material (Figure 5c), suggesting that the emplacement of fluidized ejecta sometimes triggers these flows (Figure 5b). Because these landslides appear distinct from the larger flow or ejecta and generally overprint the other materials, they appear to be secondary failures. Intermediate T2–T3 flows do appear to source from downslope areas surrounding craters. Alternatively, intermediate T2–T3 features may represent a distinct ejecta facies on Ceres in that they may be failures that form within or due to ejecta. The features shown in Figure 5 are found in Kupalo crater and are associated with fluidized appearing ejecta (e.g., Hughson et al., 2019) but clearly show distinctive toes suggestive of flows emplaced later. Additionally, Juling crater, where significant ice has been detected by Dawn's Visible and Infrared (VIR) spectrometer (Combe et al., 2018; Formisano et al., 2018), is close to this region. This collocation is consistent with a regional enhancement of near surface ice near Juling and Kupalo.

Table 1
Catalog of Intermediate Landslide Characterization

ID	Lat	Lon	Closest archetype	Description
IM001	57.819	86.110	T1	Contact cratering
IM002	34.416	37.783	T2	Failure outside of crater
IM003	66.960	26.350	T1	Small flow
IM004	66.725	25.462	T1	Secondary smaller flow
IM005	67.106	25.620	T1	Collapse crater rime outside of flow into older crater
IM006	69.920	24.783	T1	No clear rim failure
IM007	68.359	26.426	T1	Rim failure, thinner than T1
IM008	61.933	52.165	T1	Rim failure, forked deposit
IM009	58.153	56.327	T1/T2	Contact cratering
IM010	50.118	235.692	T2	Contact cratering
IM011	−50.556	3.822	T2	Degraded, thin, outside of crater
IM012	62.103	254.498	T2	Possible contact cratering
IM013	26.293	14.668	T2	Rim failure
IM014	35.261	48.523	T2	Clear point of failure, no distinct toe
IM015	32.373	47.640	T1	Not lobate, short runout length
IM016	−6.132	115.651	T1	Contact cratering
IM017	49.204	169.713	T2	Small failure outside of crater
IM018	60.027	158.114	T1	Contact cratering
IM019	52.912	146.574	T1	Contact cratering
IM020	−44.165	173.687	T2/T3	Long runout crater rim failure/ejecta
IM021	−38.253	173.127	T2	No distinct rim failure, surroundings have T3 properties
IM022	−40.666	168.397	T2/T3	T3 properties but with distinct toe feature
IM023	−35.271	168.058	T1	Juling crater
IM025	59.590	333.149	T1	Unclear failure point
IM027	29.393	308.184	T2	Multiple flows?
IM028	31.692	310.095	T1	Possible contact cratering
IM030	6.299	346.454	T2	Contact cratering
IM031	35.060	352.849	T1	Contact cratering
IM032	45.923	283.944	T1/T2	Possible contact cratering, thin but short L
IM033	12.715	335.094	T2	Contact cratering
IM034	26.180	334.200	T2	Small failures along northern rim of crater
IM035	51.734	315.255	T1/T2	Contact cratering
IM036	35.380	304.930	T1/T2	Thin, short runout length
IM037	6.618	359.360	T2	Degraded rim failure
IM038	26.754	299.325	T2	Flow inside new crater
IM039	60.776	249.026	T2	Possible contact cratering
IM040	63.314	250.549	T1	Ponded material
IM041	62.801	250.410	T1	First flow
IM042	62.811	250.058	T1	Secondary flow
IM043	18.728	234.401	T1/T3	Rounded toe, T3 environment
IM049	1.303	0.000	T1	Small flow
IM050	62.026	0.000	T3	Ejecta-like, but has definition around the flow
IM051	51.408	0.000	T1	Failure on rim noticeable, very lobate/ponded
IM052	30.151	269.024	T1/T2	No clear scar, definite deposit
IM053	−0.113	252.409	T1	Ponded material on eastern rim
IM054	1.808	251.274	T1	Very small, defined toe and lobate
IM055	64.732	282.559	T2	Multiple lobes
IM056	65.532	278.314	T2	No distinct toe
IM057	25.724	253.619	T1	Small, T3 environment but distinct lobate flow
IM058	12.500	243.911	T2/T3	Ejecta-like with defined toe
IM059	5.624	241.038	T2	Multiple lobes, small
IM060	5.483	241.025	T2	Multiple lobes, small
IM061	4.843	238.124	T1/T3	T3 environment with distinct flow
IM062	3.536	236.056	T1/T3	T3 environment with distinct flow
IM063	7.364	238.667	T1/T3	T3 environment with distinct flow
IM064	46.975	239.485	T1	Contact cratering
IM065	33.952	231.966	T2	Small
IM066	3.117	215.104	T3	Ejecta-like
IM067	3.155	0.000	T3	Ejecta-like
IM068	9.452	0.000	T2	Small contact cratering

Table 1
(continued)

ID	Lat	Lon	Closest archetype	Description
IM069	31.350	262.419	T2	Multiple flows, thin
IM070	20.849	7.933	T1	Ponded material, no clear point of failure
IM071	29.911	0.371	T1	Degraded, definite failure, deposit not well-defined
IM072	−47.668	0.000	T1/T2	Thin, yet has rounded toe
IM073	−38.587	0.000	T1/T2	Contact cratering
IM075	20.690	101.432	T1/T2	Possible contact cratering, thin but has lobate shape
IM076	6.720	88.859	T1	Possible ponded material
IM078	−35.499	167.575	T1/T2	Juling crater
IM080	−3.356	144.199	T1/T3	Small flow in T3 environment
IM081	−24.628	136.960	T2	Possible contact cratering
IM082	22.328	160.488	T2	Small deposit from contact cratering
IM083	20.248	159.686	T1/T3	Small
IM084	20.031	159.745	T2	Small
IM085	6.888	149.965	T1/T2	Thick with long runout length
IM086	−23.269	57.154	T1	Contact cratering
IM087	−42.752	45.781	T2	Degraded, thin, rounded toe
IM088	33.771	95.668	T1/T2	Thin but rounded, possibly multiple flows
IM089	37.875	86.312	T3	Possible contact cratering, ejecta like
IM090	24.185	19.119	T1	Ponded material, no clear failure point
IM091	−30.258	203.834	T2	Contact cratering
IM092	−38.531	266.392	T2	Failed ridge wall
IM093	−39.021	265.934	T2	Failed ridge wall
IM094	−39.963	265.115	T2	Failed ridge wall
IM095	−40.273	264.695	T2	Failed ridge wall
IM096	−40.873	264.186	T2	Failed ridge wall
IM097	−41.086	263.683	T2	Failed ridge wall
IM098	31.411	290.091	T1	Small
IM099	−37.330	177.154	T2/T3	Ejecta-like with defined toe
IM100	−38.568	178.237	T2/T3	Ejecta-like with defined toe
IM101	−37.607	178.663	T2/T3	Ejecta-like with defined toe
IM102	21.679	192.047	T2	Possible contact cratering
IM103	−44.578	153.337	T2	Possibly multiple flows
IM104	−40.926	111.953	T2/T3	Looks like T2 but acts like ejecta
IM106	−77.413	165.034	T1	Multiple lobate flows
IM107	−43.034	38.013	T2	Contact cratering
IM108	−34.055	90.876	T1/T2	Long runout, rounded toe
IM109	54.359	95.147	T1/T2	Contact cratering
IM110	67.998	262.797	T2	Possibly multiple flows
IM111	−53.603	275.704	T2/T3	Ejecta-like with defined toe, multiple flows
IM112	−54.894	275.384	T3	Ejecta-like
IM113	−7.604	220.524	T1	Slight rim failure, lobate
IM114	−33.714	264.401	T2/T3	Ejecta-like with defined toe, rim failure
IM115	58.520	263.129	T2	Multiple flows, defined toes

2.4. Crater Rim Mass Wasting

Mass wasting from crater rims is common across Ceres. This is generally expressed as wide debris aprons at the base of internal crater walls, where layers of loose material are gathered. In our analyses, we do not treat these as discrete landslides. However, there are features that are similar to generic mass wasting deposits but that have more discrete lobate margins that are separate from or extend outward from other debris (Figure 6), which may be the result of small-scale mass wasting or discrete landslides. In a few cases, we observe talus-like material deposits on, or just below, the crater wall, similar to other small landslides, but absent any distinct failure scarps. At the same time, these are more lobate, thicker, and more extended than other debris aprons, even within the same crater. On Earth, similar features are seen in glaciated settings called "protalus lobes" (e.g., Humlum, 2000). On Ceres, these "protalus" flows are generally very small compared to other landslides, one to seven kilometers in length and one to three kilometers in width. We have
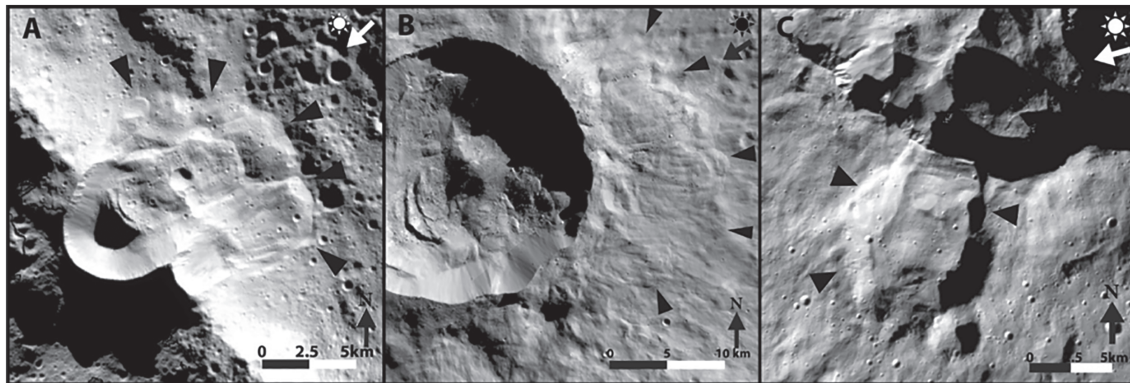
Figure 4. Multilobed landslides possess overlapping lobes and trunks. (a) [−77.413°, 165.034°] This feature, which was also described in Schmidt et al. (2017) is a result of a small impact into the rim of an older crater. There are several overlapping flows that comprise the feature, suggesting several failures, and making it challenging to assess where the maximum and center of mass measurements would be taken. (b) [−53.603°, 275.704°] The flows in Nunghui crater have morphology of both T2 and T3 flows and resemble fluidized ejecta but have a defined toe like a T2 landslide. There is not a clear scar, but the morphology is distinctive from the fluidized appearing ejecta that skirts the crater. It appears the northernmost flow occurred after the ejecta was emplaced, followed by the southern flow, which overlaps the northern lobe. It is also unclear if the flows have distal toes due to one consolidated flow or buildup of material from multiple failures. (c) [66.725°, 25.620°] A wide rim failure landslide with T1-style morphology is flanked with two smaller flows sourcing from the western side of the crater. The landslide appears to be caused by failure of the wall of the older, more degraded crater into which the deposit flowed.

included these features in our inventory of identified landslides, because the geometry of these deposits is similar to the toes of T1 flows and to those of more obvious small landslides, which is not true of other mass wasting observed on Ceres. The best example is located in the Datan crater complex, which also produced fluidized ejecta and other landslides (Figures 6a and 12). However, without an obvious source scarp or trunk, whether these features are landslides is ambiguous. It is possible that these protalus materials form from talus that slides down the crater wall as opposed to rim failure, but their horizontal extent into the crater floor is generally longer and their margins more defined than other mass wasting deposits, suggesting some amount of cohesive motion. Similar types of deposits are found in glacial settings on Earth (e.g., Humlum, 2000; Whalley & Azizi, 2003) formed from deforming ice-rich debris accumulated at the base of high topography. Thus, the morphology and locations of these lobate materials may be consistent with high ice content. Others, such as that in Figure 6c are more similar to features seen on other terrestrial bodies such as Vesta, for which a connection with subsurface ice would be unclear.
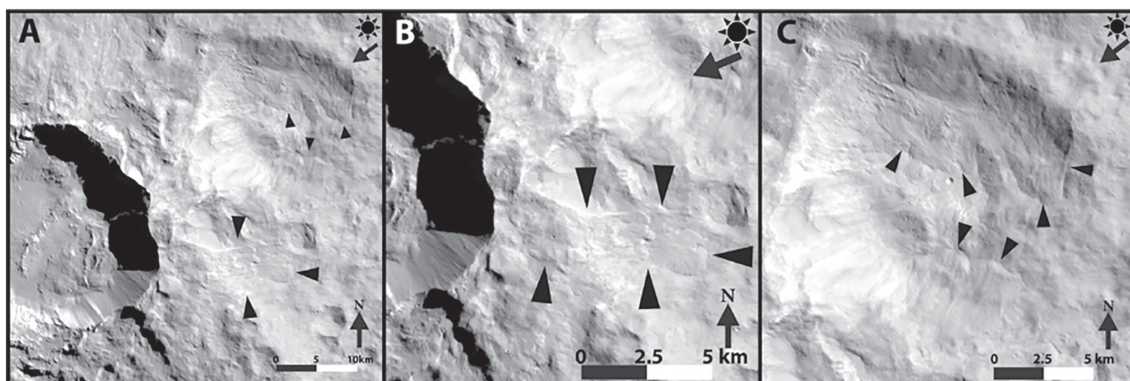

Figure 5. Ejecta-landslides are associated with or form within ejecta, as for Kupalo crater shown here. For each of these flows, there is no obvious scar to signal rim failure, which would be consistent with sourcing from or triggering by ejecta from the impact. It appears as if the Kupalo impact, lower left in (a) dispersed ejecta across the surface and onto the older crater to the east, where other ejecta and T3-like flows are seen. (b) [−40.666°, 168.397°] This set of flows resembles ejecta from the westerly crater but it has very defined toes. Multiple overlapping flows are seen. (c) [−37.330°, 177.154°] The older crater at upper right of (a) has multiple flows of fluid-like material with very defined toes sourcing all around the crater rim, but with no apparent failure suggesting a superficial nature and relationship with surrounding ejecta. The northern flows have a more angular toe and are channelized and diverted around topography (T3-like), while the southern flows appear more rounded and to flow down the rim (T2-like). Furrows along the flow path are apparent in (c) but are not as evident in (b). Kupalo's close association with Juling, which also has landslides and has spectrally detected ice, may suggest a regional enhancement of ice.
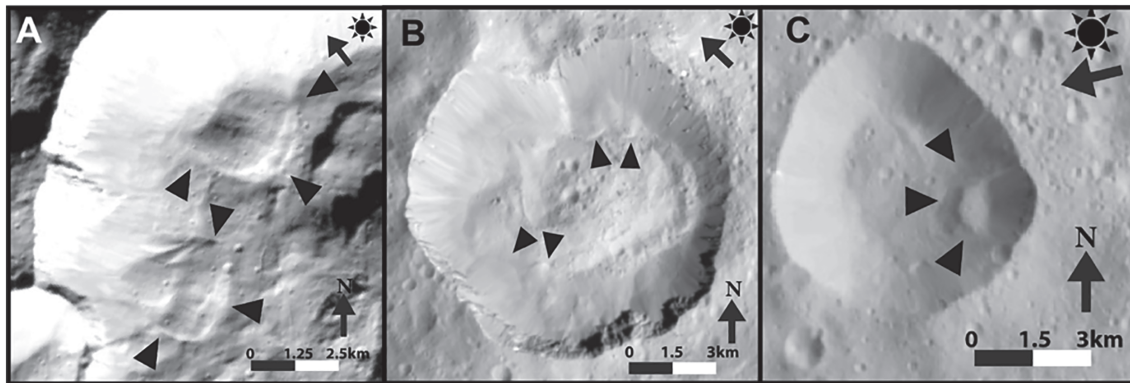
Figure 6. Protalus material forms small rounded ponds, often without defined trunks, in the base of craters. (a) [63.314°, 250.058°] Datan crater has two instances of ponded material on the northwestern rim of the small northern crater. No clear scars are present, but a distinct lobate deposit is seen. In the southern flow, two instances of ponded material overlap each other. (b) [20.849°, 7.933°] Multiple ponds of material are seen that gradate into other mass wasting; the two most prominent cases are indicated. These are much thinner deposits than typically seen for this type of feature would not be obviously different from the other mass wasting, except for the somewhat furrowed appearance and more defined toes relative to other mass wasting along the eastern rim. (c) [−0.113°, 252.409°] This feature exhibits built-up material descending from the rim of the crater. In most cases there is not a defined scar, but a defined deposit and toe are present below a semicircular section of the rim suggesting failure. It can be inferred that this failure may be caused by loosely packed material on the rim, perhaps exceeding its angle of repose, causing it to fail. Interestingly, this feature looks most like a few features seen on Vesta, which has very few landslides and none that appear fluidized.

2.5. Small Flows

Very small flows, similar in scale to the protalus deposits described above, but with defined scars and trunks, are found across Ceres. These flows, examples of which are shown in Figure 7, generally are less than 5 km long and about 3 km in length. These small trunk-shaped flows may indicate that the materials they contain flow easily since the volume of material moved is quite small, yet the deposits are relatively long and thick. The most complex of these small trunk flows is found in Oxo crater and has a T1 morphology and multiple lobes (Figure 7a). Other small trunk flows are found in the same locations as T3 flows but appear to be more lobate with a defined toe. In most instances, these flows lack a visible scar. Because of their small sizes, even the 35-m/pixel resolution of the LAMO Framing Camera images limit the interpretation of these features and may obscure any failure scarps. However, that they possess defined toes and trunks argues for cohesive motion of materials, even at small scales.

2.6. "Plains-Type" Landslides

While the majority of landslides occur within or surrounding impact craters, we have identified several examples of landslides in the plains between craters (Figure 8) and interior to catenae (Figure 9). In Figure 8, we show an example of a plains-type landslide, which has distinct T2 morphology: a wide, draped, fan-shaped deposit, longitudinal furrows along the path of motion and widening from the mouth of the flow to the toe. This plains-type flow appears channelized, typical of T2 and T3 flows, and is found within the ejecta blanket from Occator crater but overprinting the ejecta, suggesting that the flow is associated with ejecta but occurred after the ejecta was emplaced. Occator is known to be young (~20 Ma) and have a recently active crater floor (e.g., Nathues, Platz, Thangjam, et al., 2017). However, unlike the flows described above and shown in Figure 5, the ejecta in this region does not appear to be fluidized—it is absent any other lobate structures typically associated with fluidized ejecta. Rather, the radial lineation of the ejecta blanket appears ballistic in nature. Due to the low relief in the area and lack of an obvious source scar, this feature is difficult to interpret. In Figure 9, several old, degraded lobate deposits are seen flowing into the floor of Pongal Catena (Scully et al., 2017) near Urvara crater. We interpret these as landslides because of the sharp wall topography, relatively defined trunks, and rounded toes of the deposits. We identified deposits that appear to flow from distinct sources, while the scarps are degraded presumably due to age, the shape of the flows are similar to other landslides and they are found in a steeply sloping area that could promote landslides. The degraded nature of the features does not lend itself to simple measurements, nor is it possible to estimate failure conditions given the lack of distinct scars. And while failures inside tectonic features are relatively rare on Ceres, these types of valley settings are the most common on other planets—where
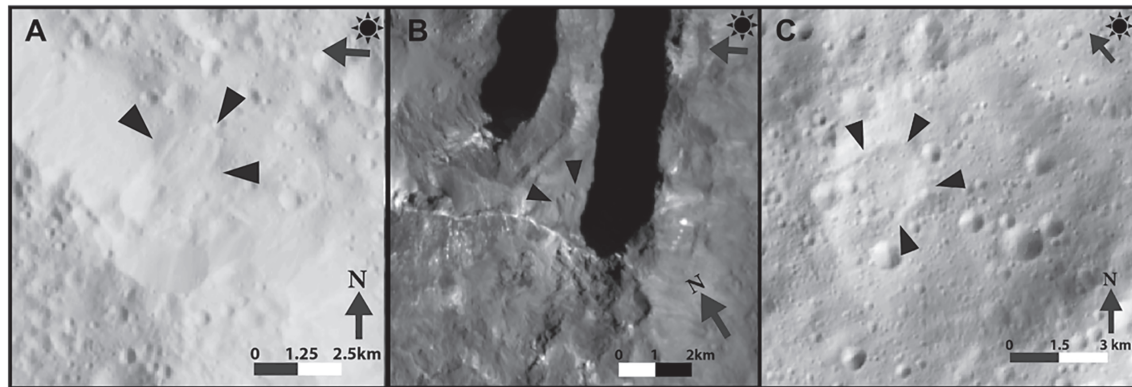
Figure 7. Small landslides have traits similar to those of larger flows, but all are under 5 km long. Small flows can be associated with both craters and fractures. For each of these flows, clear trunks or deposits clearly identify them as landslides rather than talus material. (a) [1.303°, −100.941°] In this feature a definite scar and toe is seen, for a relatively thin flow. (b) [−0.2756°, 41.504°] A small, thin failure inside Oxo. (c) [31.411°, 290.091°] This very small relatively old landslide has a scar and distinct toe with a defined but possibly deflated trunk running down the crater rim evident from shadows along its northern edge.

sharp walls fail, creating landslides (e.g., McEwen 1989; Singer et al., 2012). Ice has been detected in nearby Baltay Catena (Combe et al., 2018), and Nughui to the south of Baltay also has T2 flows and fluidized ejecta (Figures 4b and 9a), perhaps arguing for enhanced ice surrounding Urvara.

Overall, aside from landslides that occur at contact craters, we find that the bulk of the large flows described here are morphologically most similar to T2 flows (Table 1). There are very few instances of T1 flows, and these are generally easy to distinguish. Our morphological analyses support that T3 flows are associated with potentially fluidized ejecta, finding no examples of these in other settings.

3. Landslide Geometry and Mobility

A common method for obtaining information about the emplacement and characteristics of a landslide is via the ratio of its drop height, H, to its horizontal travel distance, L. Because a landslide's H/L value relates its initial potential energy to the energy dissipated by friction during transport, the ratio can be interpreted as an effective coefficient of friction and thus is a rudimentary way to describe how efficiently a landslide moves (e.g., de Blasio, 2011; Legros, 2002; Singer et al., 2012). To find the H/L value, a topographic profile was taken from the Dawn shape model (Preusker et al., 2016) across the flow, starting at the top of the scarp and stretching to the distal end of the deposit toe, and from this the drop height (H) and run-out length (L) is obtained. In some cases, where an obvious failure scarp is not present, the maximum height is taken to be the top of the crater rim. In other cases, where the toe is not clearly defined, we compared the length profile to the topography to obtain the best estimate. Chilton et al. (2019) measure both H/L (defined in that paper as H/L_{max}) and the center of mass H/L, which requires an assessment of the center of mass of the initial crater wall and deposit. In this study we measured the H/L_{max} values only, given that this paper focuses on a wide range of features where often the center of mass would not be simple to constrain and thus would introduce significant uncertainty that would be difficult to quantify. We employ H/L_{max} values to compare to the results from Schmidt et al. (2017) and the archetypal features in Chilton et al. (2019), in order to draw out any obvious differences or similarities between the intermediate landslide populations and other features. The H/L ratio is commonly used to describe both terrestrial and planetary landslides (Legros, 2002; Singer et al., 2012), and generally the maximum values are used in planetary analyses given that the data are often limited to spacecraft images often without topographic data. Thus, while H/L_{max} overestimates the total amount of kinetic energy within the flow, it is more systematic and more widely used in other work, and thus all values presented here are H/L_{max}.

In Figure 10, we present H/L_{max} values for the T1 and T2 features (Chilton et al., 2019; Schmidt et al., 2017), alongside those for the intermediate features described above and in Table 1, in which for these features we improved on our initial measurements by making several topographic profiles where possible of each feature to derive the best H_{max} and L_{max} values and computed averages (data available in Table
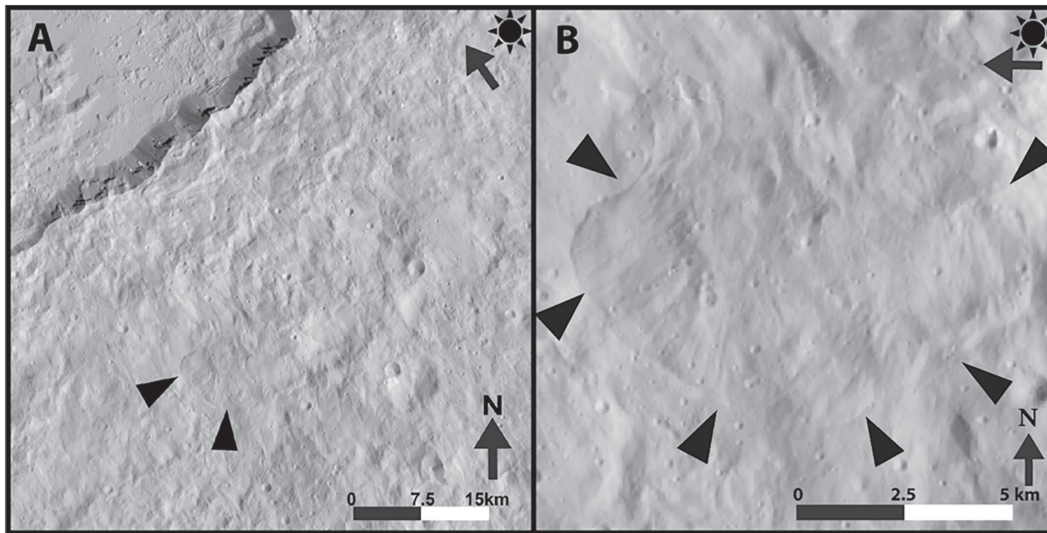
Figure 8. In rare cases, discrete flows form away from crater walls, associated with ejecta crossing broad plains. (a) [12.5°, 243.911°] Occator crater is the source of the ejecta overprinted by the flow in (b). Without an evident scar, the relationship of the flow with the ejecta suggests the landslide was triggered by the ejecta. The landslide appears to be initiated at the rim of a much older subdued crater. The feature has a distinct toe and furrows (T2-like) as well as a spreading and diversion around topography (T3-like) with a relatively short length compared to its width (T3-like). These features make it unlike the generally unorganized blanket of ballistic fluidized ejecta surrounding the crater.

S1 and Figure S1 of the supporting information). The ratio of H/L versus L is a first-order comparison that has been used to test whether there is a relationship between the friction within a flow (H/L) and the lateral transport distance (L) of the landslide. For flows governed by their own internal dissipation, H/L and L should be related (friction should be lower for flows that are longer, with a roughly linear relationship). If there is no clear relationship, this argues that the mobility of the landslide is unexpectedly high (e.g., Singer et al., 2012). In the case of ice-rich flows, this is interpreted
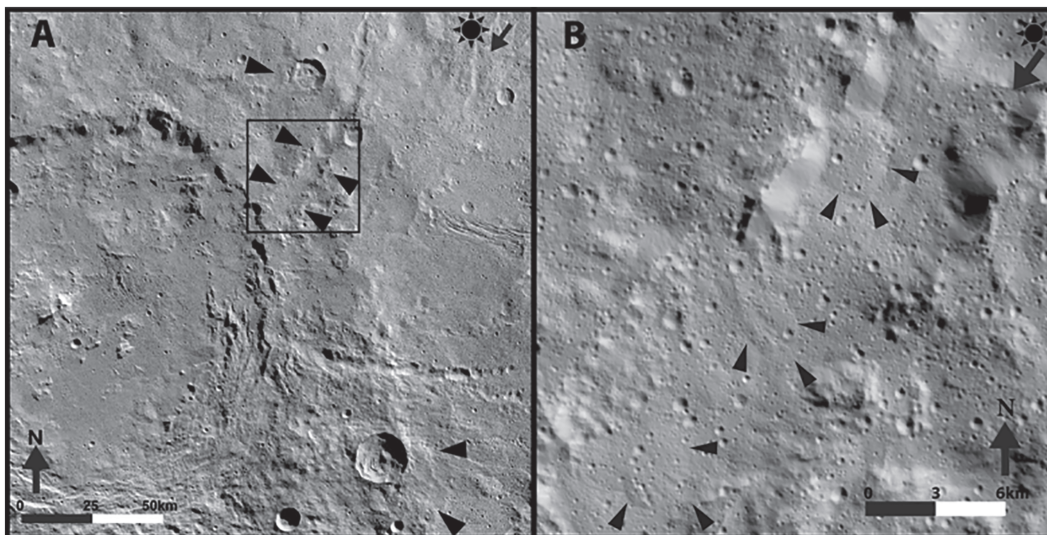

Figure 9. While most features are associated with craters, some landslides appear to have formed inside catenae such as those seen here in Pongal Catena. (a) [−33.714°, 264.401°] In this region surrounding Urvara crater, we see a series of landslides on a catena ridge (four arrows near center), a T3 flow appearing within ejecta (bottom right, [−53.603°, 275.704°]), and a T2 flow from a crater (upper middle single arrow). (b) [−39.963°, 265.115°] A series of old landslides appear to source from the walls of the catena. There are multiple sources of failure and the flows are small in size, with a few appearing to be just ponded material at the floor. Nearby Baltay Catena has exposed ice spectrally detected by VIR (Combe et al., 2018), making it plausible that this region is enhanced with ice due to the prevalence of ice-dependent features.
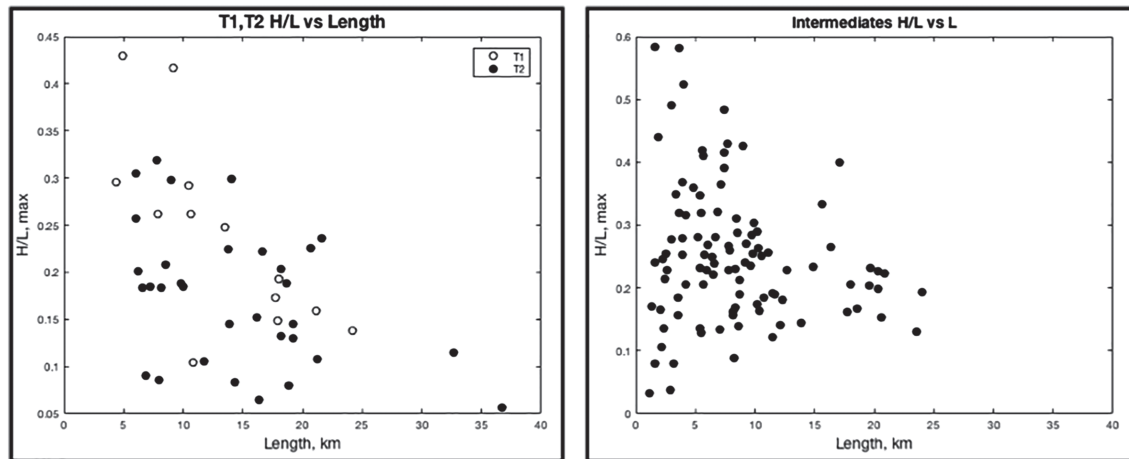
Figure 10. Despite morphological differences, trends in H/L versus L, an estimate of flow mobility, are similar between the archetype T1 and T2 flows and that observed in the intermediate landslides. For neither population is there a clear relationship between H/L and L (an R^2 value of 0.0251 for the intermediate flows).

as occurring due to ice becoming slippery or melting along grain boundaries or at the base of the flow. Figure 10 shows that there is no strong relationship between H/L and L for the intermediate flows (an R^2 value of 0.0251) nor a significant difference between the behaviors of the archetypal flows and those described here. Rather, this result supports previous conclusions that landslides on Ceres occupy a continuum of morphology but that their characteristics are consistent with flow lubrication across a wide variety of scales. Alongside the distribution of these features, this is consistent with mobilization by ice within the deposit, since the deposits travel farther than would be expected based on simple sliding mechanics.

As another possible constraint on the properties of these landslides, we also investigated whether any trends in the estimated angle of repose (AoR) of Ceres flows were evident. Materials that have exceeded their static AoR are prone to failure, conversely once these failing materials suspend motion they are said to be at their dynamic AoR, and all of these conditions depend on the grain geometry (e.g., Carrigy 1970; Kleinhans et al., 2011; Wang et al., 2013), strength and failure of surrounding topography (e.g., Culmann, 1875; Schmidt & Montgomery, 1995). To bound the AoR for the materials within landslides on Ceres, we extracted the slope of the most linear section of the topographic profile of each landslide between the failure rim and the start of the deposit (Figure S5) to represent the slope at which materials within the landslide stopped sliding, that is, the dynamic AoR. We then compared this to the crater wall slope, as reflective of the AoR prior to the failure of the landslide. We assume this failure is related to the strength of the bedrock that constructs the crater wall (Chilton et al., 2019; Schmidt & Montgomery, 1995) that might be inherited by the sliding material. We compared the slopes to explore whether the features we observe systematically derive their steepness from the geometry of the crater wall or have a different behavior that indicates a difference between the bedrock and debris. Neither H/L nor AoR are exact measurements of the nature of a landslide, however trends in these quantities are thought to derive from properties of the flow such as cohesion, friction, and sliding. For example, the AoR qualitatively assesses grain-grain interactions for quasi-granular materials (Carrigy 1970). H/L is impacted by internal friction as would come from grain boundary interactions as well as basal friction and other sources of dissipation. In the case of granular materials at the transition into sliding we would expect a close relationship between the AoR and the crater wall; we would expect a relationship between the AoR and H/L values in most landslides given that both depend on internal friction. Thus, we also investigated whether crater wall slope is the strongest control on the landslide geometry, to test whether the landslides might be well described by loose accumulation of materials along the crater wall, which did not show a clear trend (Figure S2). We found that the AoR as estimated here does not differ significantly from the H/L value for most flows, and thus, as measured here, is not a good constraint on the dynamics of landslide processes on Ceres.
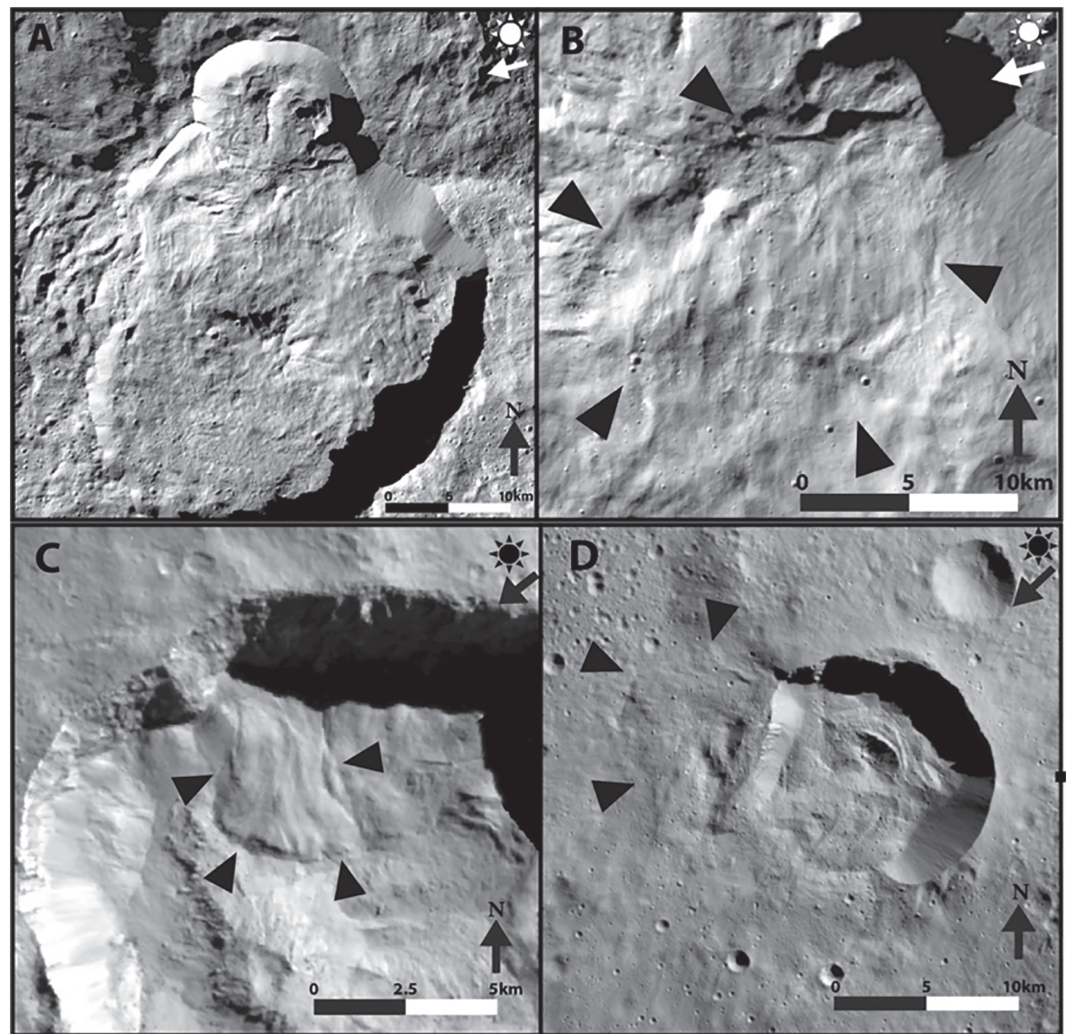
Figure 11. Morphologically anomalous flows in some cases have distinct settings and apparent flow behavior. Here, we show three examples of morphologically unique features. (a) [62.103°, 254.498°] This image of Datan crater shows the setting for the flow in (b) that occurs along the northeastern contact between the rim of the two craters. Datan crater is also the source of the widest apron of T3 landslides and fluidized appearing ejecta (Hughson et al., 2019). The landslide derives from the steep scar on the wall (shadowed region in b), with a long run out length and thin, sheeted deposit. Furrows on the surface depict the direction of motion that terminates in a lobate toe. (c) [−35.271°, 168.058°] The broad landslide in Juling crater emanates from a steep scarp rim on which ice has been detected (Formisano et al., 2018). It has a long run out length, longitudinal flow lines on the surface along the direction of motion and a define toe (T1-like), but is shallow sloping and more arcuate than other T1 flows. D) [−33.714°, 264.401°] This flow is very thin like ejecta with a moderate run out length (T2 or T3 like). While the flow resembles ejecta, it has a distinct rounded toe, and appears both younger and less diffuse that the ejecta that extends from the rim to the north and west of the flow.

4. Discussion and Conclusions

Landslides on Ceres could form due to a variety of factors—impact triggering, seismic shaking, material instability due to ice or its sublimation, etc.—and could be affected by surrounding terrain and varying basal conditions (e.g., Chilton et al., 2019; Hughson et al., 2019; Schmidt et al., 2017). As described in section 2, even within similar settings, no two landslides are completely alike. Indeed, this is why landslides are not simple to characterize individually. However, comparing features to each other, across global, regional, and local scales as well as from planet to planet does help constrain how material properties may vary and provides data by which to compare planets to each other. We describe the range in geologic setting and geomorphology in order to call out that features may appear somewhat different from each other,

even though our analysis suggests that most of these features form from common mechanisms and from similar physical properties within the subsurface.

A wide range of landslide geomorphology, failure, and emplacement behavior is observed on Ceres. The classification of T1, T2, and T3 morphology has been previously investigated as an indicator of the styles of landslide emplacement (Hughson et al., 2019; Schmidt et al., 2017) and failure and movement of landslide debris (Chilton et al., 2019). However, we have observed notable outliers to this picture, such as landslides formed in contact craters and special locations like Juling crater. For features that fall between the end member types or for which observing geometry is not well suited to more detailed measurement, comparative geomorphological analyses alongside simple geometric arguments provide an opportunity to apply lessons learned from the archetype features as well as those found on other bodies such as Mars and Enceladus to the variety of intermediate landslides we observe.

Our analysis of these features shows that the distribution of landslides along the continuum from T1 to T2 follows the same latitudinal trends as the T1 and T2 landslides, where most T1-like features are found at high latitudes and T2 at middle to low latitudes. This confirms and reinforces the conclusions found in Schmidt et al. (2017) that showed the geographic distribution of landslides is consistent with shallower ice near the poles. While some of these features share morphologic properties of both the T1 and T2 classes, the majority of the intermediate landslides are T2-like (over 40%). When comparing H/L values of the intermediate landslides to those of the T1 and T2 flows, it is apparent that there is no strong relationship between H/L and L in either group, consistent with the hypothesis that these features are lubricated by ice within the landslide debris (e.g., Schmidt et al., 2017; Singer et al., 2012). The range of H/L values for the features described here spans wider than that of the T2 and T1 landslides: The upper range (higher H/L vs. shorter L) is more comparable to the T1 flows, and the lower range to those observed for the T2 features. Interestingly, many intermediate flows appear to have longer run-out lengths than those observed in the T2 landslides.

While Hughson et al., 2019, map a few new examples of fluidized ejecta relative to that discussed in Schmidt et al. (2017), we do not find any more T3-style landslides than those observed in earlier work, all of which occur within or associated with fluidized appearing ejecta. This suggests that the conclusion of Schmidt et al. (2017) that T3 landslides derive from fluidized materials associated with impact ejecta remains consistent with geomorphic and geographic analyses at higher resolution and also suggests that there may still be a distinction between fluidized ejecta and landslides. In other words, T3 landslides may form in fluidized ejecta blankets, however, not all fluidized ejecta on Ceres produces features we would designate as landslides.

In addition to landslides that generally fit the T1-T2-T3 continuum, we also identified a few features that are physical and geomorphological outliers. Based on morphology and in some cases spectroscopy, we suspect these outlying flows to have a more heavily hydrated or ice-rich subsurface affecting their motion. Generally, these outliers have steeper crater walls, but there are examples of shallow angle flows with long extents. The most significant morphological outliers we observe belong to flows inside Juling, associated with a 25-km^2 section of exposed ice along the northern wall (Formisano et al., 2018). Thus, we interpret that at least some of the variation we observe in landslide morphology and deposit geometry is due to varying ice content.

The prevalence of T2-like features within the continuum of landslides is consistent with the analysis of Chilton et al. (2019), which argues for a layered subsurface that promotes shallow landslide failure in an ice-poor layer over most of the surface of Ceres equatorward of 50°. Special circumstances, such as a local ice layer that extends closer to the surface (e.g., at Juling and in the high latitudes) or deep excavation by impacts (in the case of contact craters) could then allow for deeper failure or anomalous landslide mobility, producing what we observe as "outlier" behavior relative to the majority of landslides. Coupled with the concurrence of landslides with surface ice (Combe et al., 2018) and other morphological features associated with ice (fluidized ejecta, pitted materials, and small-scale fractures; Sizemore et al., 2018) near Kupalo and Juling craters and near Urvara crater, our analysis is consistent with the conclusion that these regions possess particularly high ice content. Clusters of landslides and other ground ice-related features that tentatively extend from Juling, Kupalo, and Urvara through the Hanami Planum could be consistent with ice-rich highlands and thus offer a potential target for future studies of crustal ice content.

Our work suggests that the conclusions derived from analysis of the archetype features can be extended to most landslides on Ceres. Our analyses in sections 2 and 3 present more detail than Schmidt et al. (2017) but are consistent with the conclusion that landslides on Ceres are mobilized by subsurface ice. Our work demonstrates that there is not an observable difference between the physical properties, in general, of the materials involved in the formation of the vast majority of the intermediate landslides, from those that are classified as type examples. Coupled analysis of the geologic context, morphology, and emplacement style of the landslides presented here suggests that while there is significant variation between the morphology of individual landslides, overall most features behave similarly to the archetypal T1 and T2 landslides (Figure 10 and Table 1).

Data Availability Statement

The imaging data herein were taken by the Dawn Framing Camera. All raw and calibrated imaging data are available for public download in the Planetary Data System. The data behind Figures 10, 11, S1, and S2 are available in supporting information Table S1 available online, along with supporting information Figures S1–S5, via Open Science Framework: Schmidt (2019). Supporting Information for Duarte et al. 2019, JGR-Planets, L7andslides on Ceres: Diversity and Geologic Context. Retrieved online (osf.io/fgrvm). Supporting information is available online.

References

Bland, M. T., Raymond, C. A., Schenk, P. M., Fu, R. R., Kneissl, T., Pasckert, J. H., et al. (2016). Composition and structure of the shallow subsurface of Ceres revealed by crater morphology. *Nature Geoscience*, *9*(7), 538–542.

Buczkowski, D. L., Schmidt, B. E., Williams, D. A., Mest, S. C., Scully, J. E. C., Ermakov, A. I., et al. (2016). The geomorphology of Ceres. *Science*, *353*(6303), aaf4332. https://doi.org/10.1126/science.aaf4332

Carrigy, M. A. (1970). Experiments on the angles of repose of granular materials 1. *Sedimentology*, *14*(3–4), 147–158.

Chilton, H. T., Schmidt, B. E., Duarte, K., Ferrier, K. L., Hughson, K. H. G., Scully, J. E. C., et al. (2019). Landslides on Ceres: Inferences into ice content and layering in the upper crust. *Journal of Geophysical Research: Planets*, *124*, 1512–1524. https://doi.org/10.1029/2018JE005634

Kleinhans, M. G., Markies, H., de Vet, S. J., in 't Veld, A. C., & Postema, F. N. (2011). Static and dynamic angles of repose in loose granular materials under reduced gravity. *Journal of Geophysical Research-Planets*, *116*, E11004. https://doi.org/10.1029/2011JE003865

Combe, J., McCord, T. B., Tosi, F., Ammannito, E., Carrozzo, F. G., de Sanctis, M. C., et al. (2016). Detection of local H_2O exposed at the surface of Ceres. *Science*, *353*(6303). https://doi.org/10.1126/science.aaf3010

Combe, J. P., Raponi, A., Tosi, F., De Sanctis, M. C., Carrozzo, F. G., Zambon, F., et al. (2017). Exposed H_2O-rich areas detected on Ceres with the dawn visible and infrared mapping spectrometer. *Icarus*, *318*, 22–41.

Combe, J.-P., Raponi, A., Tosi, F., de Sanctis, M. C., Carrozzo, F. C., Zambon, F., et al. (2018). Exposed H_2O-rich areas detected on Ceres with the dawn visible and infrared mapping spectrometer. *Icarus*, *318*, 22–41. https://doi.org/10.1016/j.icarus.2017.12.008

Culmann, K. (1875). *Die Graphitsche Statik*. Switzerland: Meyer & Zeller.

de Blasio, F. V. (2011). *Introduction to the physics of landslides*. Dordrecht: Springer Netherlands. https://doi.org/10.1007/978-94-007-1122-8

Formisano, M., Federico, C., De Sanctis, M. C., Frigeri, A., Magni, G., Raponi, A., et al. (2018). Thermal Stability of Water Ice in Ceres' Craters: The Case of Juling Crater. *Journal of Geophysical Research: Planets*, *123*(9), 2445–2463. https://doi.org/10.1029/2017JE005417

Hayne, P. O., & Aharonson, O. (2015). Thermal stability of ice on Ceres with rough topography. *Journal of Geophysical Research: Planets*, *120*, 1567–1584. https://doi.org/10.1002/2015JE004887

Hughson, K. H. G., Russell, C. T., Schmidt, B. E., Chilton, H. T., Sizemore, H., Schenk, P. M., & Raymond, C. A. (2019). Fluidized appearing ejecta on Ceres: Implications for the mechanical properties, frictional properties, and composition of its shallow subsurface. *Journal of Geophysical Research: Planets*, *124*, 1819–1839. https://doi.org/10.1029/2018JE005666

Humlum, O. (2000). The geomorphic significance of rock glaciers: Estimates of rock glacier debris volumes and headwall recession rates in West Greenland. *Geomorphology*, *35*(1-2), 41–67. https://doi.org/10.1016/S0169-555X(00)00022-2

Landis, M. E., Byrne, S., Schórghofer, N., Schmidt, B. E., Hayne, P. O., Castillo-Rogez, J., et al. (2017). Conditions for sublimating water ice to supply Ceres' exosphere. *Journal of Geophysical Research: Planets*, *122*, 1984–1995.

Legros, F. (2002). The mobility of long-runout landslides. *Engineering Geology*, *63*(3–4), 301–331. https://doi.org/10.1016/S0013-7952(01)00090-4

McEwen, A. S. (1989). Mobility of large rock avalanches: Evidence from Valles Marineris, Mars. *Geology*, *17*(12), 1111–1114. https://doi.org/10.1130/0091-7613(1989)017<1111:MOLRAE>2.3.CO

Nathues, A., Platz, T., Hoffmann, M., Thangjam, G., Cloutis, E. A., Applin, D. M., et al. (2017). Oxo crater on (1) Ceres: Geological history and the role of water-ice. *The Astronomical Journal*, *154*(3), 13.

Nathues, A., Platz, T., Thangjam, G., Hoffmann, M., Scully, J. E. C., Steinc, N., et al. (2017). Occator crater in color at highest spatial resolution. *Icarus*. In Press, *320*, 24–38. https://doi.org/10.1016/j.icarus.2017.12.021

Prettyman, T. H., Yamashita, N., Toplis, M. J., McSween, H. Y., Schörghofer, N., Marchi, S., et al. (2017). Extensive water ice within Ceres? Aqueously altered regolith: Evidence from nuclear spectroscopy. *Science*, *355*(6320), 55–59. https://doi.org/10.1126/science.aah6765

Preusker, F., Scholten, F., Matz, K.-D., Elgner, S., Jaumann, R., Roatsch, T., et al. (2016). Dawn at Ceres—Shape model and rotational state. *47th Lunar and Planetary Science Conference Abstract #1954*, 445–446.

Roatsch, T., Kersten, E., Matz, K., Preusker, F., Scholten, F., Jaumann, R., & Raymond, C. A. (2017). High-resolution Ceres Low Altitude Mapping Orbit Atlas derived from Dawn. *Planetary and Space Science*, *140*(April), 74–79. https://doi.org/10.1016/j.pss.2017.04.008

Schmidt, B. E. (2019, August 26). Supporting information for Duarte et al. 2019, JGR-Planets, Landslides on Ceres: Diversity and Geologic Context. Retrieved from osf.io/fgrvm

Schmidt, B. E., Hughson, K. H. G., Chilton, H. T., Scully, J. E. C., Platz, T., Nathues, A., et al. (2017). Geomorphological evidence for ground ice on dwarf planet Ceres. *Nature*, (April, *10*(5), 338–343. https://doi.org/10.1038/ngeo2936

Schmidt, K. M., & Montgomery, D. R. (1995). Limits to relief. *Science*, *270*(5236), 617–620. https://doi.org/10.1126/science.270.5236.617

Schorghofer, N., Mazarico, E., Platz, T., Preusker, F., Schróder, S. E., Raymond, C. A., et al. (2016). The permanently shadowed regions of dwarf planet Ceres. *Geophysical Research Letters*, *43*, 6783–6789.

Schröder, S. E., Maue, T., Gutiérrez Marqués, P., Mottola, S., Aye, K. M., Sierks, H., et al. (2013). In-flight calibration of the Dawn framing camera. *Icarus*, *226*(2), 1304–1317. https://doi.org/10.1016/j.icarus.2013.07.036

Schröder, S. E., Mottola, S., Matz, K.-D., & Roatsch, T. (2014). In-flight calibration of the Dawn framing camera II: Flat fields and stray light correction. *Icarus*, *234*, 99–108. https://doi.org/10.1016/j.icarus.2014.02.018

Scully, J. E. C., Buczkowski, D. L., Schmedemann, N., Raymond, C. A., Castillo-Rogez, J. C., King, S. D., et al. (2017). Evidence for the interior evolution of Ceres from geologic analysis of fractures. *Icarus*, *44*(19), 9564–9572. https://doi.org/10.1002/2017GL075086

Singer, K. N., McKinnon, W. B., Schenk, P. M., & Moore, J. M. (2012). Massive ice avalanches on Iapetus mobilized by friction reduction during flash heating. *Nature Geoscience*, *5*(8), 574–578. https://doi.org/10.1038/ngeo1526

Sizemore, H., Schmidt, B. E., Chilton, H. T., Hughson, K. H. G., Platz, T., Sori, M., et al. (2018). Ice-related morphological features on dwarf planet Ceres: Distribution and Implications for the Global Cryosphere. *Journal of Geophysical Research: Planets*, *124*, 1650–1689. https://doi.org/10.1029/2018JE005699

Wang, J.-J., Zhao, D., Liang, Y., & Wen, H.-B. (2013). Angle of repose of landslide debris deposits induced by 2008 Sichuan Earthquake. *Engineering Geology*, *156*, 103–110. https://doi.org/10.1016/j.enggeo.2013.01.021

Whalley, W. B., & Azizi, F. (2003). Rock glaciers and protalus landforms: Analogous forms and ice sources on Earth and Mars. *Journal of Geophysical Research*, *108*(E4), 8032. https://doi.org/10.1029/2002JE001864